Large-Eddy Simulation for Golf Ball Aerodynamics: The effect of surface roughness on the drag crisis and the Magnus effect

Jing LI
Graduate School of Engineering
Hokkaido University
N13 W8, Kita-ku, Sapporo, Japan
jingli@eis.hokudai.ac.jp

Makoto TSUBOKURA
Department of Computational Science, Graduate School of System Informatics, Kobe University, and RIKEN Advanced Institute for Computational Science
1-1 Rokkodai, Nada-ku, Kobe, Japan
tsubo@tiger.kobe-u.ac.jp

Masaya TSUNODA
Research & Development HQ
Sumitomo Rubber Industries Ltd.
2-1-1 Tsutsui-cho, Chuo-ku, Kobe, Japan
m-tsunoda.az@srigroup.co.jp

Jun IKEDA
Graduate School of Engineering
Hokkaido University
N13 W8, Kita-ku, Sapporo, Japan
z-ikeda@mech-hm.eng.hokudai.ac.jp

Introduction

The game of golf, first played almost six hundred years ago in Scotland, is one of the most popular sports all around the world. Among the physics hiding behind the game, the most interesting one relating to fluid dynamics is the aerodynamics of the golf ball. Two important factors to explain the aerodynamics are the surface roughness created by dimples and ball's self-rotation. The former is discussed in terms of the enhancement of the drag crisis, which drastically decreases the aerodynamics drag and stabilizes the flight path. On the other hand, the latter affects the flight distance of the ball through the additional lift force created by the Magnus effect. These two factors are supposed to interact with each other through the transition of surface boundary layer and sensitively affect the separation and reattachment points. While optimization of the dimple pattern of the golf ball is still one of the main design factors in its manufacturing process, its detailed physical mechanisms of how the dimple contribute to reduce the drag (Choi et al., 2006; Smith et al., 2010) and affect the Magnus effect (Muto et al., 2012) have not yet been fully understood. Accordingly the objective of this study is, by conducting the Large-Eddy Simulation of fully resolving the surface boundary layer, to investigate the effect of surface roughness on the drag crisis and the Magnus effect through the comparison of the smooth and dimpled rotating sphere at around critical Reynolds number.

Target Geometries and Simulation Conditions

Geometry details of the golf ball used in the present study as the roughness sphere model are shown in Fig.1. The dimensionless geometry parameter k/D quantitatively measures the roughness of a golf ball, where k is the dimple depth and D represents the diameter of the spheres, and is approximately 0.5×10^{-2} for our golf ball model. Muto's sphere model (Muto et al., 2012) is used as the corresponding smooth sphere in the present study. In order to properly reproduce the drag crisis, the Reynolds numbers with respect to the sphere diameter and approaching flow velocity are set to be 4.3×10^{4}, 7.5×10^{4} and 1.1×10^{5} respectively for the subcritical, critical and supercritical golf ball cases. The spin parameter Γ defined as the ratio of the ball's surface rotating velocity ($\omega D/2$ where ω is the angular velocity of rotation) and the approaching flow velocity is set to be equal to 0.1, considering the real golf boll's flight condition.

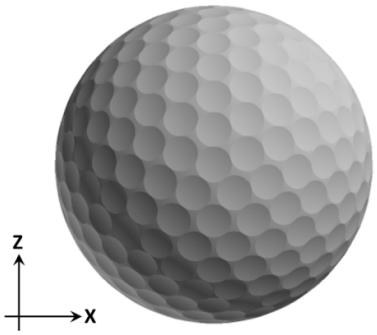

Figure 1: Geometry of golf ball

Numerical Methods and Mesh Generation

The spatially filtered Navier-Stokes equations were discretized based on the vertex centered finite volume method for fully unstructured grids, considering the flexibility of the uniform grid resolution on the surface and precise reproduction of the dimple shape. The dynamic subgird-scale eddy viscosity model by Germano et al. (1991) was adopted. The second order central difference scheme was used for the spatial derivatives, while 5% of the first order upwind scheme was blended for the calculation of convection term to avoid unexpected numerical oscillation. For the rotating cases, in order to reproduce the self-rotation of the golf ball, entire flow filed was rotated without changing its coordinate fixed on the inertial frame of reference. This strategy satisfactorily solved the challenge to properly reproducing the change of boundary configuration with respect to the incoming flow direction while the golf ball is rotating. To impose a rotating motion on the flow field, arbitrary Lagrangean-Eulerian (ALE) method was adopted (Hirt et al., 1974). This method allowed instantaneously moving vertexes to the new positions determined according to the specific spinning conditions.

The surface of the balls was reproduced by uniform triangle meshes and prism layers were allocated along the normal-wall direction starting from the surface mesh to resolve the boundary layer. The required grid resolution was estimated based on the laminar boundary-layer thickness δ_B on the surface estimated by Shlichting (1955) (Muto et al., 2012; Li et al., 2014). For the golf ball case at the highest Reynolds number considered in the present study, the near-wall resolution was finally determined to be approximately 1/34 δ_B for the thickness of the first prism layer on the surface and around 1/3 δ_B for the directions parallel to the solid surface (see Fig.2 in the case of golf ball). The total mesh number amounts to about 150 million.

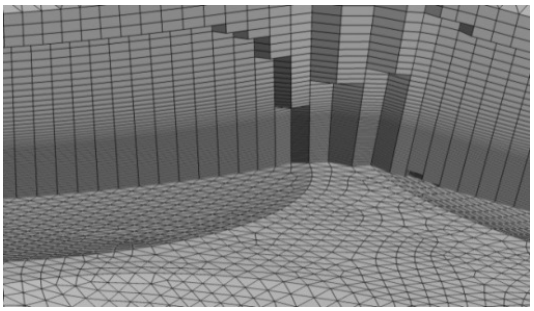

Figure 2: Numerical meshes around the surface of golf ball

Results and Discussions

Fig.3 plots the numerical results of drag coefficients for the present non-rotating golf ball cases and Muto's non-rotating smooth sphere cases (Muto et al., 2012). The experimental data obtained in the previous literatures including both the stationary golf balls and smooth spheres (Wieselsberger, 1922; Achenbach, 1972; Choi et al., 2006) are also shown in Fig.3 as references. As indicated in this figure, the drag crisis of the present golf ball model has been successfully reproduced in our simulations, such that the drag coefficient stays at about 0.49 at the subcritical Reynolds number (Re=4.3 $\times 10^4$) and decreases sharply to around 0.22 at the supercritical Reynolds number (Re=1.1 $\times 10^5$), and our results show a good agreement with the experimental data obtained by Choi et al. (2006). It is also clearly shown in fig.3 that the drag crisis occurs at a remarkably lower Reynolds number for the present golf ball compared with the smooth spheres, even though the discrepancy between the drag coefficients of the golf ball and the smooth spheres is limited at the subcritical Reynolds numbers.

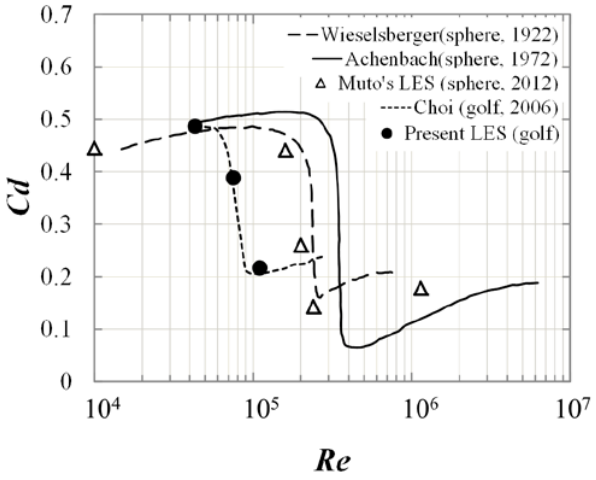

Figure 3: Drag coefficient in the stationary cases

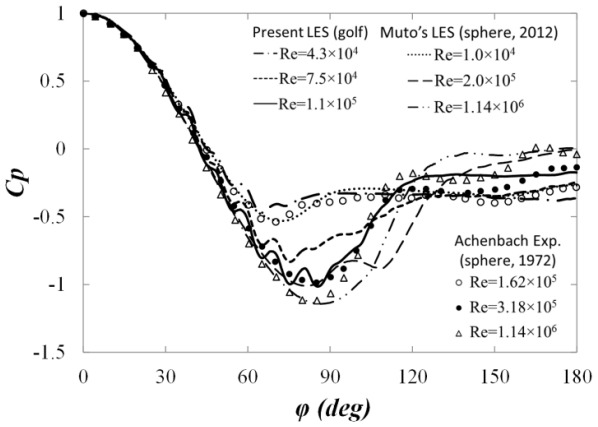

Figure 4: Surface pressure distributions in the stationary cases

The statistics of the mean pressure distribution on the stationary golf ball surface are plotted in Fig.4, with both Muto's numerical results (Muto et al., 2012) and Achenbach's experimental data (Achenbach, 1972) for the non-rotating smooth spheres being included as references. The polar angle φ in the figures is measured from the front stagnation point. Specifically, the data for golf ball cases are obtained along the central joint line of the golf ball. Such path doesn't go across any of the dimples on the surface. One can observe from fig.4 that the pressure distribution on the golf ball surface at the subcritical Reynolds number ($Re=4.3\times10^4$) is similar to the corresponding distributions of the smooth spheres in the same regime. For both the golf ball and the smooth spheres, the pressure profile drops remarkably in the critical regime due to the transition from laminar boundary layer to turbulent boundary layer and the consequent delay of flow separation. At the supercritical Reynolds number ($Re=1.1\times10^5$), the pressure profile of the golf ball appears to be comparable to the experiment data of the smooth sphere obtained at $Re=3.18\times10^5$ (Achenbach, 1972) in terms of the minimum pressure value and its angular position. Moreover, the C_p value of the golf ball shows some local changes in several angular positions. Such variation is mainly affected by the local pressure distribution inside the dimples in the vicinity of the central joint line.

The iso-surface of vortical flow structures around the smooth sphere and golf ball in the stationary case is provided in Fig.5 using the Q-criterion method proposed by Hunt et al (1988). One can see that for the smooth sphere shown in Fig.5 (a), which exhibits a laminar boundary layer separation at φ=87°, the flow turns to become more turbulent in the shear layer after the complete separation and vortex structures form distinctly. Similar features can be also observed for the golf ball case at the subcritical Reynolds number, as shown in Fig.5 (c), in which the flow appears to stay smooth before separation at φ=75° even there are dimples distributed on the surface, suggesting a limited perturbation of the surface roughness to the flow in the subcritical regime. However, the influence of dimples on the flow appears to be more evident in the supercritical regime. As can be seen in Fig.5 (d), at the supercritical Reynolds number, the flow becomes turbulent when it traverses dimples, and small-scale vortices are generated inside dimples. Due to the perturbation caused by the surface roughness introduced by dimples, the momentum of the near-wall flow around the golf ball is increased, which makes the flow be able to travel further downstream until complete separation at φ=105°. And this occurs at a relatively low Reynolds number compared to the smooth sphere case, in which the turbulent boundary layer with high momentum is achieved at higher a supercritical Reynolds number and consequently delays the full flow separation at φ=102°, as shown in Fig.5 (b).

Fig.6 visualizes the instantaneous wake flow structures respectively for the supercritical smooth sphere case and the supercritical golf ball case. It can be clearly observed from the wake flows that both the smooth sphere and the golf ball experience large-scale vortex shedding. An interesting phenomenon is that, especially for the smooth sphere, the wake flows show some deviation from the streamwise axis going across the centers of the spheres. Actually the statistics of the instantaneous aerodynamic forces in the supercritical regimes also indicate a nonzero lateral force exerted on both the stationary smooth sphere and the stationary golf ball, although the magnitude of the lateral force is to some extend suppressed in the golf ball case. This is also suggested by the wake structures in Fig.6, in which a less twisted flow pattern compared with the smooth sphere is shown behind the golf ball.

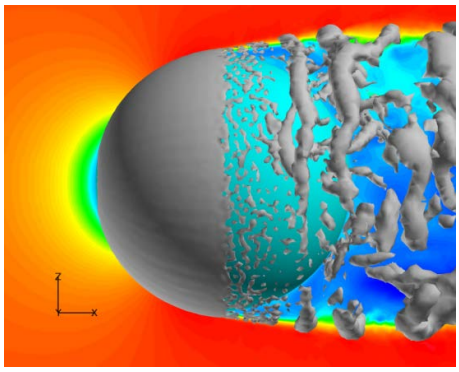

(a)

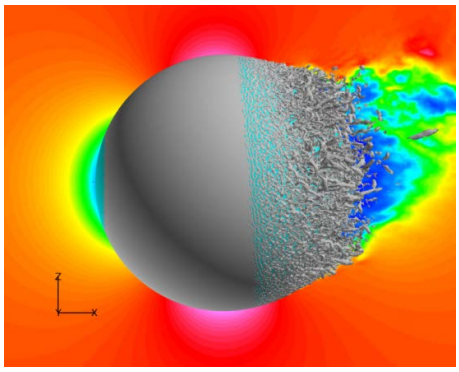

(b)

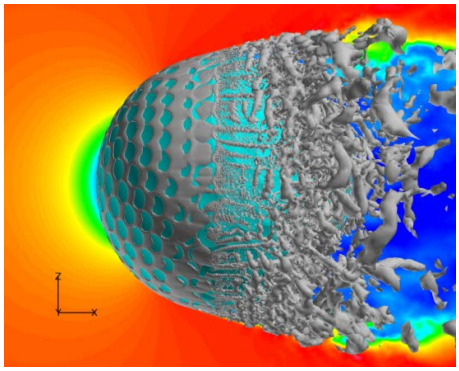

(c)

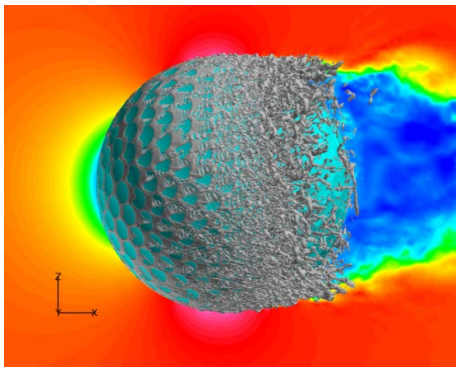

(d)

Figure 5: Flow structures (Q) around the smooth sphere and golf ball in the stationary cases: (a) Smooth at $Re=1.0\times10^4$ (before the crisis); (b) Smooth at $Re=1.14\times10^6$ (after the crisis); (c) Golf ball at $Re=4.3\times10^4$ (before the crisis); (d) Golf ball at $Re=1.1\times10^5$ (after the crisis)

(a)

(b)

Figure 6: Wake flow structures behind the smooth sphere and golf ball in the stationary cases viewed on the x-z plane, (a) Smooth at $Re=1.14\times10^6$ (after the crisis); (b) Golf ball at $Re=1.1\times10^5$ (after the crisis)

When self-rotating motion is imposed on a sphere/cylinder, it is well known that a certain amount of lift force acts on the sphere/cylinder depending on its spinning speed, which is called Magnus effect. It is explained based on the potential flow theory, while there is always discrepancy between the theoretical and actual values. The discrepancy is usually discussed with the sensitivity of the separation point of the boundary layer. The extreme case can be observed at around the critical Reynolds number where the direction of the lift force becomes opposite to the theoretical direction at specific rotational speed. This phenomenon is called negative/inverse Magnus effect. Muto et al. (2012) has conducted LES of rotating sphere and successfully reproduced negative Magnus effect at around the critical Reynolds number under certain rotating conditions. In the present study, particular attention was paid to the spinning spheres at the supercritical Reynolds numbers.

Fig.7 displays the supercritical flow fields around the spinning smooth sphere ($Re=1.14\times10^6$) and the spinning golf ball ($Re=1.1\times10^5$) respectively. The instantaneous variables shown in this figure are the pressure distribution on the surfaces of the spheres and the velocity distribution in the flow fields. The incoming flow shown in this figure goes from left to right, and the spheres are rotating clockwise around y axis with the spin parameter $\bar{I}=0.1$, thus the force pointing to the direction parallel to z axis is defined as the lift force.

The time-averaged drag and lift coefficients for the smooth sphere case shown in Fig.7 are 0.219 and 0.213 respectively. For the golf ball case, correspondingly, the time-averaged drag and lift coefficients are respectively 0.239 and 0.129. Particularly, for both the smooth sphere and the golf ball, the drag coefficients obtained under spinning condition are slightly higher than the ones in stationary cases. This phenomenon might be attributed to the changes of the wake flow patterns. Concerning the lift force, one can easily conclude based on the statistic data that, at current spinning speed, positive lift forces are exerted on both the rotating smooth sphere and golf ball in the supercritical regime. This is also visually evidenced in Fig.7, in which one can clearly observe that the wake flows in both cases are declining downwards, suggesting a lift force pointing to +z direction. However, it is interesting that the lift force value is comparable to the drag force value in the smooth sphere case, whereas in the golf ball case, the lift force appears to be nearly 50% smaller than the corresponding drag force. This may suggest lift force suppression for the spinning golf ball as well as the stationary golf ball.

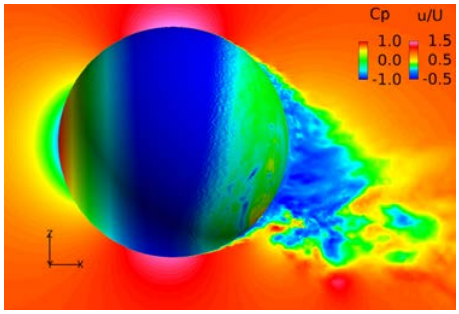

(a)

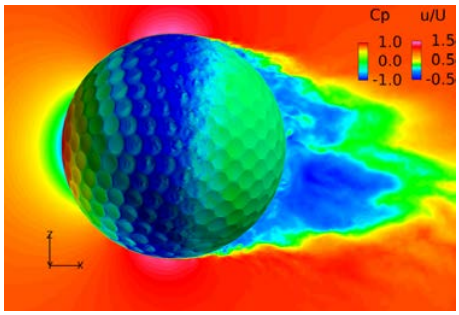

(b)

Figure 7: Flow field around the spinning smooth sphere and golf ball with spin parameter Γ=0.1, (a) Smooth at Re=1.14×10^6 (after the crisis); (b) Golf ball at Re=1.1×10^5 (after the crisis)

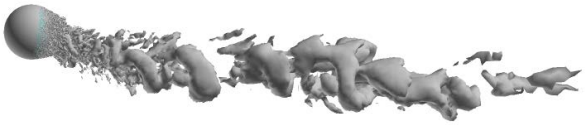

(a)

(b)

Figure 8: Wake flow structures behind the spinning smooth sphere and golf ball with spin parameter Γ=0.1 viewed on the x-z plane, (a) Smooth at Re=1.14×10^6 (after the crisis); (b) Golf ball at Re=1.1×10^5 (after the crisis)

Further insights into the wake flow structures behind the rotating spheres are displayed in Fig.8 using the Q-criterion method. Obviously, there is large-scale vortex shedding behind both the rotating smooth sphere and golf ball with hair-pin structures forming in the wake flow areas some distance away from the spheres, as in the stationary cases. Particularly, for both cases, the small-scale vortex are evident before the complete flow separation from the spheres, indicating a turbulent boundary layer on both the forward rotating (above in the figure) and backward rotating sides, which may be one of the main reasons that explains the positive direction of the lift forces.

Conclusions and Future Plan

In the present study, the flow past a golf ball and a smooth sphere has been numerically analyzed under both the stationary and spinning conditions. Particular attention was paid to the supercritical cases. The simulation result shows that the drag crisis of the golf ball occurs at a remarkably lower Reynolds number compared with the smooth sphere. This phenomenon is due to the local flow separation above the golf ball dimples and the consequent delay of the complete flow detachment. With the spin parameter Γ=0.1, both the rotating smooth sphere and golf ball experience a slightly larger drag force compared with the stationary cases and a positive lift force at the supercritical Reynolds numbers. The lift force exerted on the spinning golf ball appears to be somewhat suppressed, compared to the smooth sphere. Such a phenomenon is also observed in the stationary cases. For the next step, simulations will be conducted for self-rotating cases at various Reynolds numbers around the critical area. How the dimples affect the generation of negative lift force will be further discussed.

References

Achenbach, E, 1972, “Experiments on the flow past spheres at very high Reynolds numbers”, *J. Fluid Mech.*, vol. 54, pp.565-575.

Choi, J., Jeon, W. and Choi, H., 2006, “Mechanism of drag reduction by dimples on a sphere”, *Phys. Fluids*, vol. 18, 041702.1-041702.4

Germano, M., Piomelli, U., Moin, P. and Cabot, W.H., 1991, “A dynamic subgrid-scale eddy viscosity model”, *Phys. Fluids*, A3, pp.1760-1765.

Hirt, C.W., Amsden, A.A. and Cook, J.L., 1974, “An Arbitrary Lagrangian-Eulerian Computing Method for All Flow Speeds”, *Journal of Computational Physics*, 14, pp. 227-253.

Hunt, J.C.R., Wray, A.A. and Moin, P., 1988, “Eddies, Streams, and Convergence Zones in Turbulent Flows”, *Center for Turbulence Research Report*, CTRS88, pp. 193-208.

Li, J., Tsubokura, M. and Tsunoda, M., 2014, “Numerical investigation of drag crisis of a sphere and the effect of surface roughness”, *10th Int. ERCOFTAC Symposium on Engineering Turbulence Modelling and Measurements*, Marbella, Spain.

Muto, M., Tsubokura, M. and Oshima, N., 2012, “Negative Magnus lift on a rotating sphere at around the critical Reynolds number”, *Phys. Fluids*, vol. 24, 014102.1-014102.15.

Schlichting, H., 1955, “Boundary Layer Theory”, New York, McGraw-Hill.

Smith, C.E., Beratlis, N., Balaras, E., Squires, K. and Tsunoda, M., 2010, “Numerical investigation of the flow over a golf ball in the subcritical and supercritical regimes”, *International Journal of Heat and Fluid Flow*, Vol. 31, pp. 262-273.

Wieselsberger, C., 1922, “Weitere Feststellungen uber die Gesetze des Flussigkeits und Luftwiderstandes”. *Phys. Z.* 23, 219-224.